Role of E-Cadherin in Membrane-Cortex Interaction Probed by Nanotube Extrusion

Erdem Tabdanov,[†] Nicolas Borghi,[‡] Françoise Brochard-Wyart,[‡*] Sylvie Dufour,[†] and Jean-Paul Thiery[†]
[†]Unite Mixte de Recherche 144 and [‡]Unite Mixte de Recherche 168, Centre National de la Recherche Scientifique-Institut Curie, Paris, France

ABSTRACT This study aims to define the role of E-cadherin (Ecad) engagement in cell-cell contact during membrane-cortex interaction. As a tool, we used a hydrodynamic membrane tube extrusion technique to characterize the mechanical interaction between the plasma membrane and the underlying cortical cytoskeleton. Cells were anchored on 4.5 μm beads coated with polylysine (PL) to obtain nonspecific cell adhesion or with an antibody against Ecad to mimic specific Ecad-mediated cell adhesion. We investigated tube length dynamics $L(t)$ over time and through successive extrusions applied to the cell at regular time intervals. A constant slow velocity was observed for the first extrusion, for PL-attached cells. Subsequent extrusions had two phases: an initial high-velocity regime followed by a low-velocity regime. Successive extrusions gradually weakened the binding of the membrane around the tube neck to the underlying cortical cytoskeleton. Cells specifically attached via Ecad first exhibited a very low extrusion velocity regime followed by a faster extrusion regime similar to nonspecific extrusion. This indicates that Ecad strengthens the membrane-cortical cytoskeleton interaction, but only in a restricted area corresponding to the site of contact between the cell and the bead. Occasional giant "cortex" tubes were extruded with specifically anchored cells, demonstrating that the cortex remained tightly bound to the membrane through Ecad-mediated adhesion at the contact site.

INTRODUCTION

Cell adhesion is known to play a key role in determining embryo shape. The body plan is achieved through tight spatiotemporal regulation of adhesive mechanisms during cell sorting and tissue remodeling. Adhesive processes have been analyzed extensively during all phases of embryonic development. Cell adhesion contributes to all primary cell processes, including cell proliferation, survival, migration, and differentiation, by regulating gene expression. Cell adhesion is also a key part of adult homeostasis and plays well-established roles in immune responses, inflammation, and tissue repair. Cadherins are the major receptors controlling intercellular adhesion (1,2). Members of the cadherin superfamily play key roles in controlling cell shape and polarity. Classical cadherins are transmembrane adhesion receptors that mediate homophilic *trans* interactions between cells via their extracellular domain. The cytoplasmic domains of classical cadherins transmit adhesive signals by recruiting β-catenin, α-catenin, and eplin proteins, facilitating binding to cortical actin microfilaments (3). These adhesive complexes also contain signaling molecules and other actin-binding proteins involved in actin cytoskeleton dynamics (for review (4–6,7)). The lateral clustering of cadherins and their association with other receptors in the membrane, together with the recruitment of enzymatic and structural partners, promote the formation and regulation of specialized cell membrane domains, such as neuronal synapses (8), adherent junctions, and desmosomes (9–11 and 12). The expression of various cadherin subtypes promotes specific cell sorting (13,14 and 15) and intercellular adhesion of variable strength, as shown by measurements of separation force (16). E-cadherin (Ecad)-mediated adhesion is considerably strengthened by connection to the actin cytoskeleton (17). In cell monolayers, cadherins are not uniformly distributed along the intercellular boundaries, but instead form supramolecular adhesive clusters enriched in actin microfilaments (4,18). Although the intercellular boundaries are highly dynamic, the adhesion complexes enable the cells to remain connected during contact remodeling and are often the last structures to be disrupted during cell rounding before detachment or dispersion from monolayers (19).

Mechanical connections occur between the plasma membrane and the underlying cytoskeleton through discrete membrane-cortex binders. One of the well-described membrane-cortex binders is ezrin. Ezrin is a multidomain protein that, after activation, can bind PIP2 at its amino-terminus and actin at its carboxy-terminus (20). The amount of PIP2 in the cell is enough to completely seal the plasma membrane-cortex against the outward pressure, working to inflate the membrane (21,22). Actin cortex-plasma membrane coupling through ezrin occurs through several relatively weak, albeit dynamic, actin-ezrin-PIP2 interactions. The membrane-cortex coupling appears to be essential for control of the lateral diffusion of receptors (23,24), membrane dynamics and endocytosis (22), cell division, cytoskeletal organization, cell spreading, and cell sorting (25–27). However, the role of these connections in cadherin-mediated cell adhesion remains unclear (3,28). To investigate this coupling, a cellular peeling test based on the extrusion of membrane tubes can be used. Membrane tubes or tethers (also known as retraction fibers

Submitted June 11, 2008, and accepted for publication November 24, 2008.

*Correspondence: francoise.brochard-wyart@curie.fr

Nicolas Borghi's present address is Dept. of Biology, Stanford University, Stanford, California.

Jean-Paul Thiery's present address is Institute of Molecular and Cell Biology, A* STAR, Proteos, Singapore.

Editor: Petra Schwille.

0006-3495/09/03/2457/9 $2.00

doi: 10.1016/j.bpj.2008.11.059

(26)) may be formed during the remodeling or disruption of cell-matrix adhesion or intercellular adhesion (29) (Y. S. Chu, UMR 144, personal communication, 2005), and clusters of adhesion complexes can be found at the tip of these membrane tubes. Since the publication of Hochmuth et al.'s (30) pioneering work, tube extrusion has been widely studied in diverse cell types, including erythrocytes (31–33), neutrophils (34–36), neurons (37), and hair cells (38). It is now clear that membrane tether extrusion involves the detachment of the membrane from the cortex (31,39,40). The extrusion force can be expressed as follows (41):

$$f^3 - ff_0^2 = (2\pi)^3 2k^2 \nu \eta_e \dot{L} \ln R/r_c, \quad (1)$$

where f_0 is the static extrusion force (22), k is the membrane curvature modulus, ν is the density of membrane/cortex binders (we can estimate $\nu \sim 10^{14}$ m^{-2} from the typical mesh size of the cortex (42)), η_e is the surface viscosity associated with lipid permeation through membrane proteins bound to the cortex and the slippage of the membrane on the cortex (43), $\dot{L}$ is the extrusion velocity, R is the radius of the cell, and r_c is the radius of the proximal region near the neck of the tube in which cortex-binding membrane proteins are detached at higher extrusion velocities (see below and Fig. 6). From Eq. 1, one can derive the membrane/cortex adhesion energy from f_0, and the friction of lipids through the binders, leading to a measurement of their density ν.

Cadherin-mediated intercellular adhesion induces local changes in cortex organization. We aimed to determine the extent to which cadherins affect mechanical links between the membrane and cortex from tube extrusion dynamics. We used a hydrodynamic technique to extrude tubes from S180 cells or cells stably expressing Ecad. The cell was anchored to an adherent microbead held by a micropipette, and subjected to flow in a microchannel. As the Stokes friction force carried the cell away, a membrane tube attached to the bead was extruded from the cell body. This hydrodynamic extrusion technique can be used to extrude tubes at a wide range of forces without the need for a force transducer (30). We compared tube extrusion from cells anchored to the bead via 1), nonspecific electrostatic interactions; and 2), Ecad-specific binding.

MATERIALS AND METHODS

Cell lines

Ecad and Ecad-Δcyto cells are S180 cells that are stably transfected to produce Ecad and Ecad without its cytoplasmic domain, respectively. Ecad cells have been described elsewhere (44). The parental S180 cells do not express cadherin and do not exhibit any intercellular adhesion. Cells were cultured at 37°C under an atmosphere containing 5% CO_2 in Dulbecco's modified Eagle's medium (DMEM; Invitrogen, Carlsbad, CA) supplemented with 10% fetal bovine serum (FBS; Invitrogen, Carlsbad, CA), 2 mM glutamine, 100 U/mL penicillin, and 100 μg/mL streptomycin. Confluent cultures were routinely split after treatment with 0.05% trypsin + 0.02% EDTA in PBS. Before tube extrusion experiments were performed, the cells were isolated as previously described (45,46). They were treated with trypsin-calcium buffer (0.01% trypsin type XI (Sigma) + 10 mM calcium) and dissociated into single cells by pipetting. The single cells were resuspended in working medium (CO_2 independent medium (Invitrogen) containing 1% FBS) for immediate use.

Cell-bead complex preparation

We used 4.5 μm beads (Dynabeads, M-450 goat anti-mouse IgG; Dynal ASA, Oslo, Norway), coated with specific antibodies recognizing the extracellular domain of Ecad: 7D6 monoclonal antibody (Developmental Studies Hybridoma Bank, Iowa City, IA) for Ecad cells or ECCD2 rat monoclonal antibody (Takara, Shiga, Japan) for Ecad-Δcyto cells. Blocking antibodies have been shown to mimic the adhesive activity of cadherin (47) and can trigger cadherin-mediated cortical cytoskeleton reorganization. We used polystyrene beads with a diameter of 4.5 μm (Polybead; BioValley, Alsace, France) incubated for 40 min in 0.01% poly-L-lysine solution (Sigma, St. Louis, MO) for nonspecific cell adhesion. Cells were incubated with beads in working medium at 37°C for 40 min before the experiment.

Hydrodynamic tube extrusion

Glass micropipettes were prepared from glass capillaries with a horizontal laser pipette puller (P-2000; Sutter Instruments, Novato, CA). Tips were cut and fire-polished to give an internal diameter of 3 μm, using a forging machine (Micro Forge MF-830; Narishige Scientific Instruments Laboratory, Tokyo, Japan).

The microchannel was assembled from a transparent groove-molded sheet of polydimethylsiloxane (PDMS) and a glass coverslip. The channel (section ~150×10^{-3} mm^2, length ~1 cm) was immersed in and filled with working medium in a petri dish and connected to a motorized pumping syringe, providing a controlled flow velocity. Experiments were carried out at a temperature of 37°C, maintained using the built-in heating stage of the microscope (Leica, Weitzlar, Germany).

A hydraulic micropipette micromanipulator (Narishige Scientific Instruments Laboratory, Tokyo, Japan) was used to introduce cell-bead complexes into the microchannel, where they were subjected to flow at $U = 400$ μm/s for nonspecifically anchored cells and $U = 500$ μm/s for cells specifically anchored to the beads via Ecad. In these conditions, the Reynolds number is Re < 1, inertia can be neglected, and the extrusion force equals the friction force on the cell. The friction force is given by the Stokes relationship: $f = 6\pi\eta R(U - \dot{L})$, where η is the surrounding water viscosity, R is the cell radius, and $\dot{L}$ is the cell velocity. In general, $\dot{L}$ does not exceed 10% of U, so friction force is assumed to depend weakly on extrusion velocity, giving $f = 80$ pN. The extrusion force is thus simply proportional to the flow velocity U. Tube extrusion dynamics were monitored by transmission microscopy and recorded on videotape with a CCD camera (Sony, Tokyo, Japan). The sequences of interest were digitized and analyzed using Scion Image software (Scion, Frederick, MD).

Each cell was subjected to a hydrodynamic flow at constant velocity U. During flow, the cell is carried away at a velocity$\dot{L}$, the tube extrusion velocity. A membrane tube of length L anchors the cell to the bead held by the micropipette (Fig. 1). As the flow U is stopped, the tube retracts and the cell is pulled back to the bead. This process was repeated for n cycles of applied hydrodynamic flow at identical and constant velocity U, separated by a resting interval of 30 s, until the tube broke. The membrane into the tube comes mainly from the reservoir of membrane located in the wrinkles and cell surface microprotrusions.

RESULTS

Nonspecific cell anchorage

Parental S180 cells attached to polylysine (PL)-coated beads were subjected to cyclic tube extrusion. Tube length L is

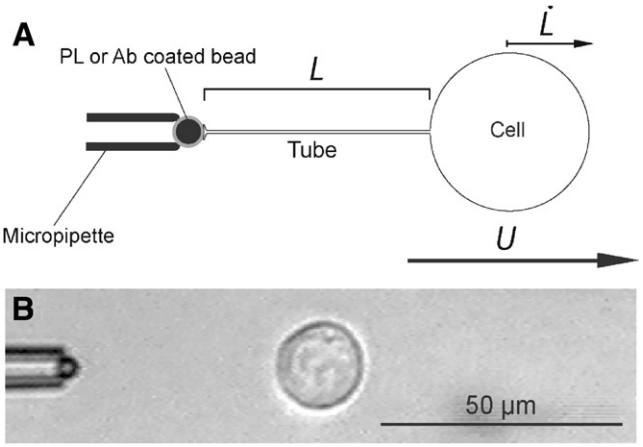

FIGURE 1 Diagram (*A*) and videomicrograph (*B*) of a tube extrusion from an S180 cell. The anchored bead is held by a suction micropipette and is coated with either PL or an antibody specific for Ecad, inducing cortical cytoskeleton reorganization. The membrane tether is not visible under these experimental conditions. The variable of interest is the velocity of tube extrusion ($\dot{L}$) at the observed tube length (L).

plotted against time for each extrusion cycle n in Fig. 2 *A*. For the first cycle, $n = 1$, the extrusion profile was frequently approximately linear. With increasing n, we observed an increase in extrusion velocity during an initial stage of tube extrusion (first regime (FR)), which was followed by a second regime (SR) of lower extrusion velocity (Fig. 2 *D*). We increased the maximal length of the extruded tubes gradually, within the cycle number n, to avoid occasional tube ruptures during the extrusion cycle, which were otherwise frequent. FR extrusion velocity and FR/SR transition tube length $L_{(FR/SR)n}$ increased progressively with n (Fig. 2, *D* and *G*), whereas SR extrusion velocity remained approximately constant (Fig. 2 *D*). Thus, tube extrusion at cycle n affected the integrity of cortex/membrane coupling over a limited cell surface area proportional to the surface of extruded tube of length $L_{(max)n}$. This can be detected by the linear correlation between the previously extruded tube length $L_{(max)n-1}$ and the transition length between FR and SR at the following cycle $L_{(FR/SR)n}$ (Fig. 3 *A*).

We investigated the possible effects of Ecad molecules that were not involved in specific adhesion at the cell surface by studying cells that produced Ecad anchored on PL-coated beads. The Ecad-producing cells behaved in a manner qualitatively similar to that of S180 cells, with two successive extrusion regimes FR and SR (Fig. 2 *B*). The FR velocity increasing with n (Fig. 2 *E*) and a similar correlation between $L_{(FR/SR)n}$ and $L_{(max)n-1}$ (see Fig. 3 *B*) is similar.

Thus, cortex/membrane coupling was similar in the two cell clones when cadherins were not involved in cell-bead adhesion.

Ecad-specific anchorage

We assessed the effect of membrane/cortex coupling involving Ecad-mediated adhesion, using Ecad cells anchored to specific antibody-coated beads.

We distinguished two major groups of cells on the basis of differences in behavior from the first cycle of extrusion. In one group (Fig. 4 *A*, *Peak 2*), tube extrusion velocity was within the same range as extrusion velocities for the nonspecifically anchored cells (Fig. 4 *B*). This pattern is referred to hereafter as the regular resistance (RR) regime. By contrast, the other group (Fig. 4 *A*, *Peak 1*) displayed an additional very slow extrusion velocity regime (referred to hereafter as the high resistance (HR) regime). This regime was followed by a faster extrusion velocity regime similar to the RR regime (Figs. 4 *A*, *inset*, and 5 *A*). The HR regime was also observed in subsequent cycles (Fig. 5 *B*). The transition length between these two regimes was ~4.2 μm for both cycles 1 and 2 (Fig. 5 *C*).

We further assessed the role of the cytoplasmic domain of cadherins in the development of the HR regime by studying cells that produced a mutant form of cadherin with a deletion in the cytoplasmic domain (Ecad-Δcyto cells) anchored on specific antibody-coated beads. The tube extrusion dynamics of these cells did not differ significantly from those of nonspecifically anchored cells (Fig. 2, *C* and *F*). Thus, the cytoplasmic domain of the Ecad molecule is clearly required for the observed increase in resistance of the cell to tube extrusion.

DISCUSSION

Progressive release of membrane binding

As shown in a previous study on red blood cells (31), for a constant extrusion velocity, the membrane flow from the cell body to the tube can be divided into two distinct regions: a distal permeation region and a proximal sliding region. In this model, which can be applied to various cell types (41), the flow velocity of lipids decreases with increasing distance from the tube neck (Fig. 6 *A*). In the distal region, lipids flow at a low velocity and do not damage the membrane/cortex binders. Lipids flow by permeation through the network of binders, leading to considerable viscous dissipation. In the proximal region, near the neck of the tube, lipid velocity is high enough to break the bonds between the membrane and the cytoskeleton; both lipids and binders slip on the cortex, resulting in a small contribution to viscous dissipation (Fig. 6 *B*).

Coupling between the membrane and cytoskeleton is intact before tube extrusion begins. The first tube extrusion is therefore governed by permeation in the distal region and accompanied by the detachment of binders in the proximal region, resulting in roughly linear tube growth, as observed in Fig. 2, *A–C*, with no distinguishable regimes (Fig. 2, *D–F*). During tube retraction, the extruded membrane flows back into the cell body. If binders remain bound during extrusion, the cell returns to its initial state. Conversely, if binders are detached in the proximal region, the retracted membrane is only partially attached close to the tube neck. The cortex is a dynamic structure, so only a fraction of binders reassociate during the short Δt interval. The development of FR may be

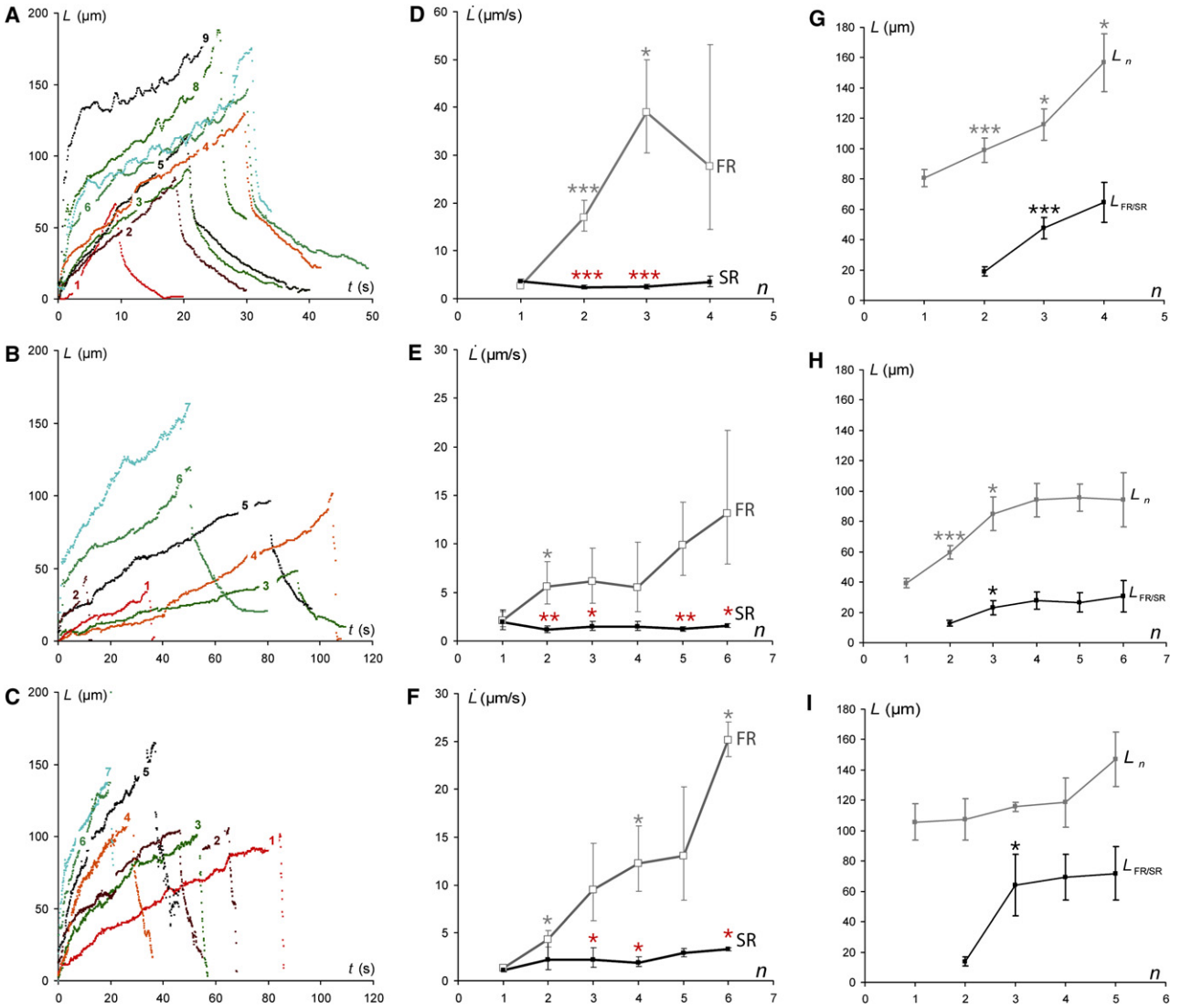

FIGURE 2 Plots of tube length against time for successive extrusion-retraction cycles separated by 30 s intervals. Numbers on profiles correspond to cycle number. (*A*) PL-anchored S180 cell. (*B*) PL-anchored Ecad cell. (*C*) Ecad-Δcyto cell anchored via antibodies specific for the extracellular domain of Ecad. Extrusion velocity is plotted against cycle number n for FR rates (□) and SR rates (■) for S180 (*D*), Ecad (*E*) and Ecad-Δcyto cells (*F*). (*G–I*) FR to SR transition tube length $L_{FR/SR}$ and the average of maximal tubes lengths for Ecad, S180, and Ecad-Δcyto cells, respectively, versus n. The midpoint in the transitional tube length interval was used as the transition point (30, 35, and 12 cells tested, respectively). Error bars represent the standard errors. *** $p < 0.001$, ** $p < 0.01$, and * $p < 0.06$. The red asterisk marks the statistical difference between the FR and SR of the same cycle. The black and gray asterisks mark the statistical difference between values of the cycle n with $n-1$ (*D–G*) or with the first cycle (*H* and *I*).

accounted for by the incomplete reestablishment of membrane-cytoskeleton binding during the 30-s interval between extrusion cycles. Moreover, as shown in Fig. 2, *A* and *B*, and Fig. S1 in the Supporting Material, tube retraction slows down with increasing cycle number n. Furthermore, tube retraction is clearly incomplete (retraction reaching zero velocity for nonzero tube length) for $n \geq 5$ (see Fig. 2, *A–C*, and Fig. S1). The decrease in tube retraction velocity reflects a decrease in retraction force, possibly accounted for by a decrease in tube membrane tension over successive cycles. This decrease in tube membrane tension may result from incomplete membrane reincorporation and its gradual accumulation within a growing proximal zone, in which the membrane remains partially detached.

In this context, the increase in extrusion velocity $\dot{L}_{FR}^{Y}$ and transition length $L_{(FR/SR)n}$ with n indicates that membrane/cortex coupling is affected in two ways over successive extrusion cycles: 1), the membrane cytoskeleton binder density in the proximal region gradually decreases (see Fig. 6 *B*, *arrows*); and 2), the growth of this zone is proportional to the length of the previous tube (as shown in Fig. 3).

Extrusion velocity remains fairly constant during the SR regime (see Fig. 2, *D–F*) and tube lengths overlap in this regime during serial extrusion (see Fig. 2, *G–I*). Thus, once

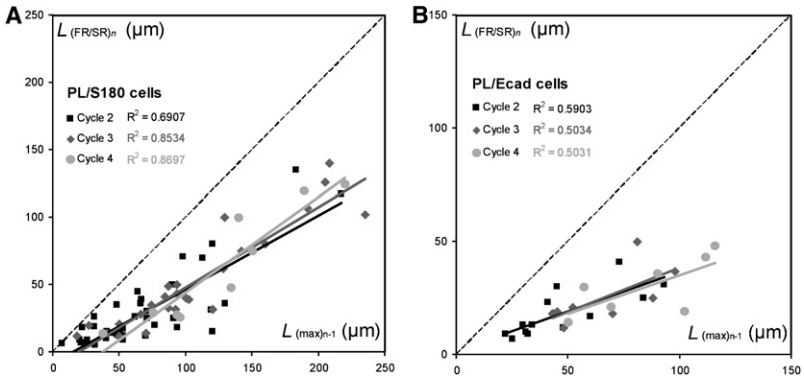

FIGURE 3 Correlation between $L_{(max)n-1}$ of cycle n-1 and the length of transition between FR and SR $L_{(FR/SR)n}$ of cycle n for S180 (*A*) and Ecad cells (*B*), attached to PL-coated beads. As shown by the linear fit, $L_{(FR/SR)n}$ is smaller but proportional to $L_{(max)n-1}$ (39 S180 cells and 13 Ecad cells tested).

the reservoir of membrane that is weakly attached to the cortex has been extruded during the FR regime, subsequent extrusion is governed by the permeation of lipids through the distal region, unaffected by previous extrusions.

Taking into account that f remains constant during all the cycles n, one can deduce the evolution of the binders' density from Eq. 1 by comparing the velocity of extrusion for FR and SR regimes. Eq. 1 gives $v_n = v_0\,\dot{L}_0/\dot{L}_n$ (see Fig. 7). It is clear

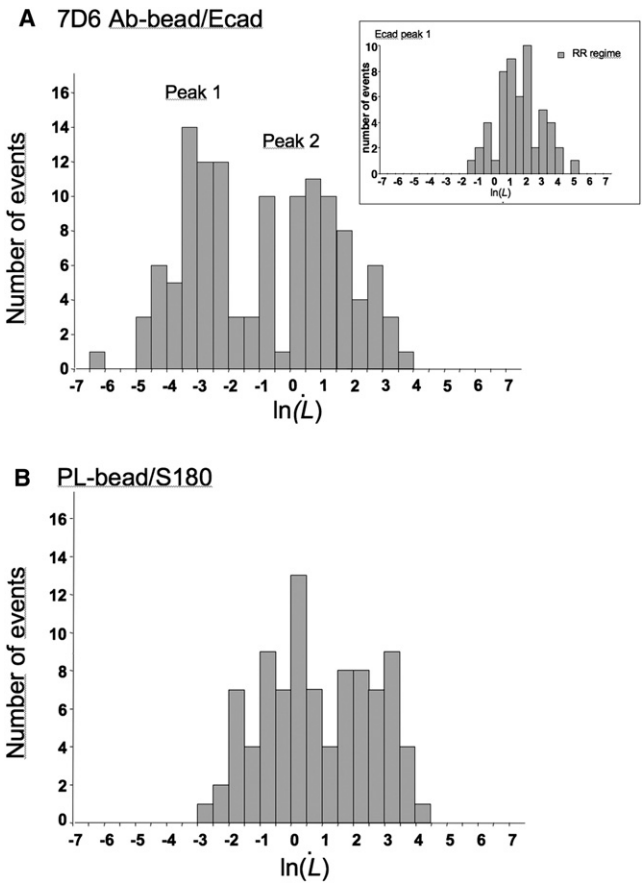

FIGURE 4 Comparison of extrusion velocity distribution for Ecad cells anchored to 7D6-coated beads (*A*) and for S180 cells anchored on PL-coated beads (*B*) at the first cycle. The distribution of the extrusion velocities measured for specifically anchored Ecad cells reveals two peaks. Peak 2 is localized at the same velocity range as the peak observed for the nonspecific anchorage. Peak 1 shows the group of specifically anchored Ecad cells displaying a very slow extrusion velocity regime (HR) during the initial phase of tube extrusion, which is followed by a faster extrusion velocity regime RR (*inset* in *A*) similar to that of the nonspecific anchorage.

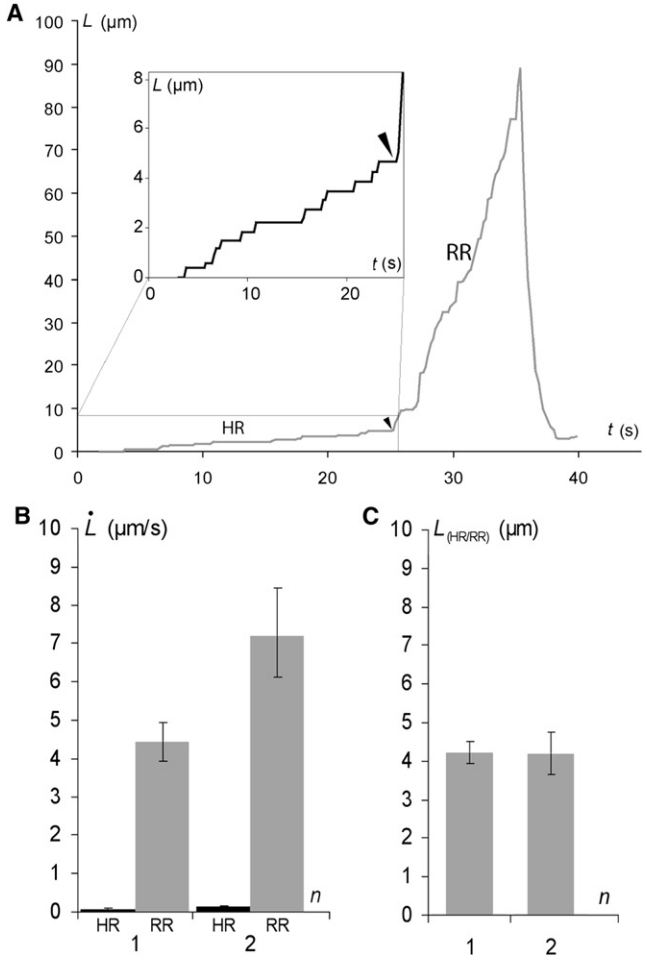

FIGURE 5 (*A*) Plots of tube length against time for an Ecad cell/Ecad bead extrusion exhibiting HR and RR regimes (first cycle). (*Inset*) Detailed tether extrusion profile for the HR regime. The arrowhead indicates the transition from highly resistant to regular resistant tether extrusion. (*B*) Tether extrusion rates for the HR and RR regimes for cycles 1 and 2. (*C*) Transition point $L_{(FR/SR)n}$ between HR and RR regimes for cycles 1 and 2. Error bars represent the standard errors (120 cells tested).

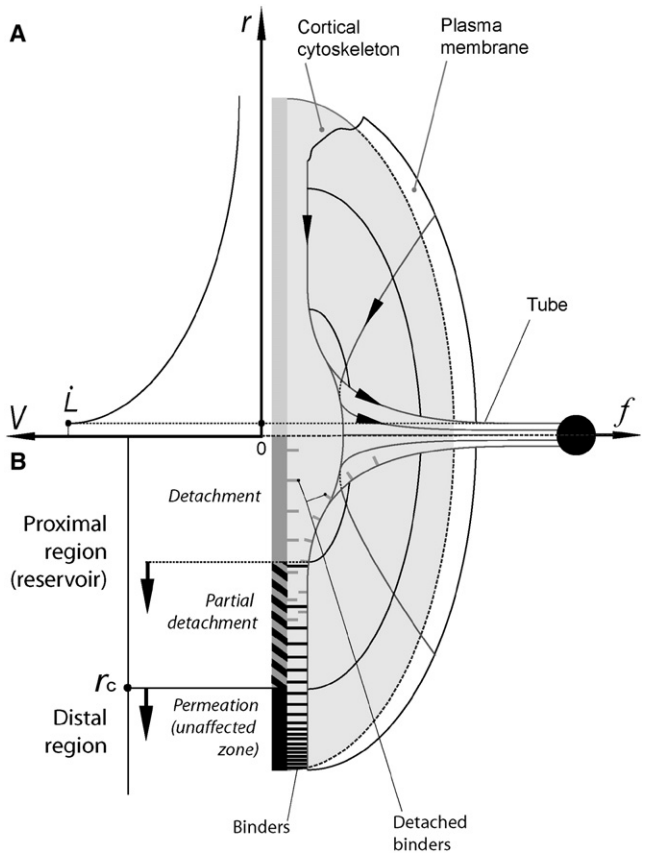

FIGURE 6 Schematic diagram of a cross section of the tube extrusion site. Lipid flow field $V(R)$ at the tube neck (A) and model of the membrane/cortical cytoskeleton interaction modes at the proximal and distal regions around the extruded tube (B). The proximal region consists in a partially detached plasma membrane surface, surrounded by the intact distal region. The proximal region grows with cycle number (*arrows*).

that ν_n falls by a large factor after the first extrusion and less for the following extrusions. As ν_n decreases, the friction on the binders decreases and the tear out is reduced or stopped.

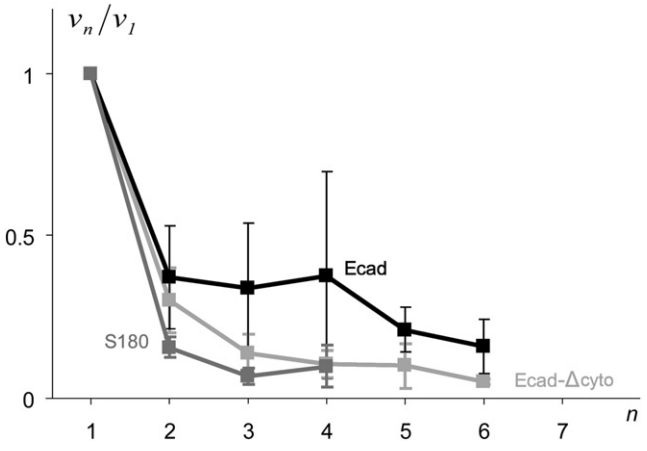

FIGURE 7 Plot of the $\dot{L}^{Y}_{FR(1)}/\dot{L}^{Y}_{FR(n)} \cong \nu_n/\nu_1$ ratio (normalized binder density; ν_1 is the density of binders in the first cycle, and ν_n is the density of binders for cycle n). The ratio decreases with cycle number for S180 cells/PL-beads, Ecad cells/PL-beads, and Ecad-Δcyto/Ab-beads.

In addition to extrusions at a time interval $\Delta t = 30$ s, we also performed extrusions at higher Δt values. For time intervals of 2 min between extrusion cycles, extrusion did not become easier over successive cycles, as reported for $\Delta t = 30$ s (Fig. S2), indicating that the membrane reattaches to the cortex within 2 min.

Role of specific adhesion

The strengthening of Ecad-mediated cell-cell contact has been shown to reach a plateau at ~40 min (46). We allowed cell-bead contact to develop for 40 min before performing the extrusion experiments, to prevent excessive scattering of results due to the development of cell-bead adhesion complexes.

Extrusion cycles with a higher flow velocity ($U = 500$ μm/s) were required for successful tube extrusion in a significant number of trials when the cells were anchored via specific cadherin interactions. Cortex/membrane adhesion energy was therefore higher than that for the nonspecific adhesion case. We usually first observed a very low extrusion velocity regime (HR) with high resistance to tube extrusion (Fig. 5 *A*), up to a tube length $L_{HRn} \sim 4.2$ μm (Fig. 5 *C*). Based on these data, we can estimate the cortex area restructured by interaction with Ecad. Assuming the membrane tube diameter $d \sim 30$ nm (d is derived from the classical relation $d = 4\pi k_m f^{-1}$, where k_m is the membrane curvature modulus of order 50 kT (30),), we obtain a surface area ~0.4 μm^2. In addition, step-like tube growth was observed during the HR regime, suggesting a strong disturbance of lipid flow in this region (Fig. 5 *A*, *inset*).

These observations indicate that Ecad-mediated cytoskeleton modification is a local phenomenon, and that membrane flow is strongly disturbed in Ecad-specific adhesion patches. Local Ecad-mediated cytoskeleton modification may reflect the ability of cells to adapt to the microenvironment with a very high degree of spatial accuracy, allowing them to integrate very fine spatial adhesion cues to establish morphological features, such as neuronal synapses (8). The HR regime may be interpreted as a progressive disruption of the strong cadherin-cortex connection. The force corresponding to the step-like tube growth is used to detach the membrane from the tightly associated underlying cortex, using an energy W_{cad}. W_{cad} can be estimated from the conservation of energy $fL = \pi d L W_{cad}$. With f, the Stokes force = 80 pN for $U = 500$ μm/s, and $d \sim 30$ nm, it gives $W_{cad} \sim 0.8$ mN/m. This energy is much greater than the typical nonspecific membrane/cortex energy, which we have deduced from the measurement of f_0, the static extrusion force, and is on the order of 0.1 mN/m (Fig. S3) (35,48). It is interesting to compare this value with the energy of rupture of Ecad cell doublets measured in dual pipette assays. For a rupture force $f_R = 200$ nN, the intercellular adhesion energy W can be estimated at 8 mN/m using de Gennes's formula $f_R = \pi R W$, where R is the cell radius. It has been shown that the cadherin-cytoskeleton coupling is crucial (46). W is divided by a factor of 50 for mutated cadherins (Ecad-Δcyto cell doublets) (see (50)).

By contrast, the extrusion velocity for the RR regime was in the same range as that for PL-mediated anchored cells (Fig. 4 and Fig. S4). We detected an increase in $\dot{L}^{Y}_{RR}$ with increasing n, consistent with a similar pattern of a progressive degradation of membrane/cortex coupling (see Fig. 5 *B*). However, extruded tubes for cells specifically anchored via Ecad were more fragile than nonspecifically anchored Ecad cells. The mean maximum tube length before rupture was shorter than for the other cases (see Fig. 8 *A*). This phenomenon was accompanied by frequent tube disruptions, limiting the mean number of tubes per cell to two (Fig. 8 *B*). These observations reveal a correlation between high resistance to lipid flow and tube fragility. The second tube extrusion also displayed an HR regime, suggesting that Ecad-mediated cortex adhesion to the membrane recovered after the first cycle of extrusion and retraction (Figs. 4, *C* and *D*, and 5 *B*). The half-life of cadherin-catenin-cytoskeleton complexes has not been established; however, these complexes may be highly dynamic, as cadherin and actin have half-lives of ~10 s (49), suggesting that these complexes may reform rapidly after binder detachment.

Alternatively, upon Ecad-mediated cell/bead contact, the membrane pulling may result in the formation of a cortical tube. We observed this phenomenon in a minority of cells (eight of the 93 cells tested) that formed short giant tubes of radius r_c with a length of ~2 μm (see Fig. 9). The formation of such protrusions suggests that these tubes are ''cortex'' tubes. They demonstrate strong binding of the bead to the cortex via cadherin molecules. Assuming that the cortex behaves like a viscoelastic sheet, we can estimate a curvature modulus k_c from $r_c = \sqrt{k_c/2\sigma_c}$ (53), where σ_c is the cortical tension. Using $\sigma \sim 3 \times 10^{-5}\,\mathrm{Nm}^{-1}$, a typical value for cortical tension (51,52), and $r_c = 2\ \mu$m, we obtain $k_c \cong 2.4 \times 10^{-16} J$, which is a thousand times larger than the membrane curvature modulus. This value of k_c corresponds to the curvature modulus of a shell of elastic modulus E on the order of 10^4 Pa (54,55) and thickness h on the order of 0.5 μm ($k_c \sim Eh^3/9$ (56) for an incompressible layer).

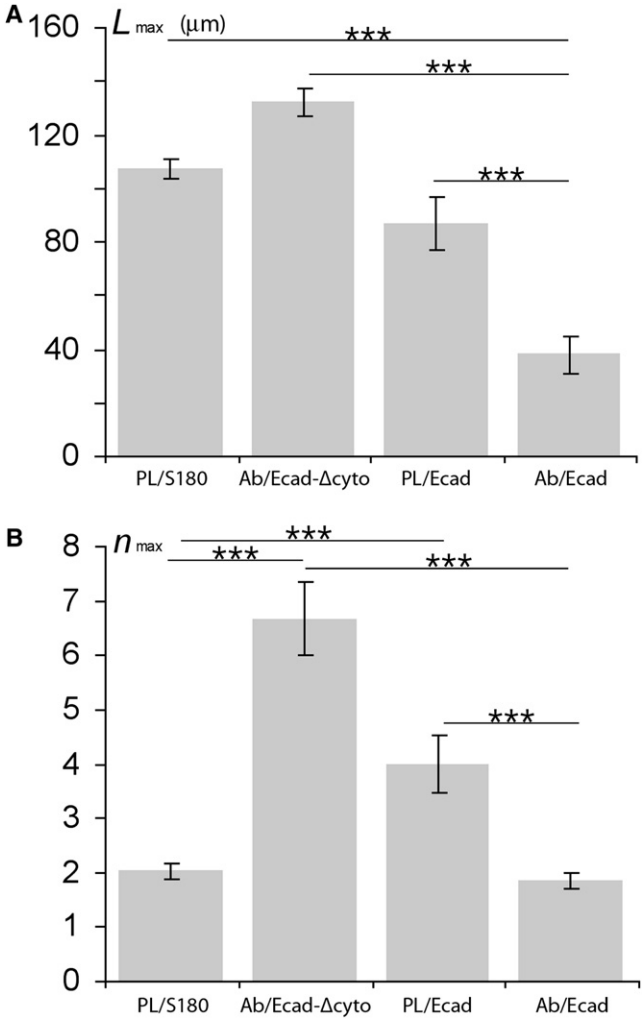

FIGURE 8 Mean tube length (*A*) and mean extrusion cycle number (*B*) before tube rupture for S180 and Ecad cells/PL-beads, and for Ecad and Ecad-Δcyto cells/Ab-beads. Error bars represent the standard errors. *** $p < 0.001$.

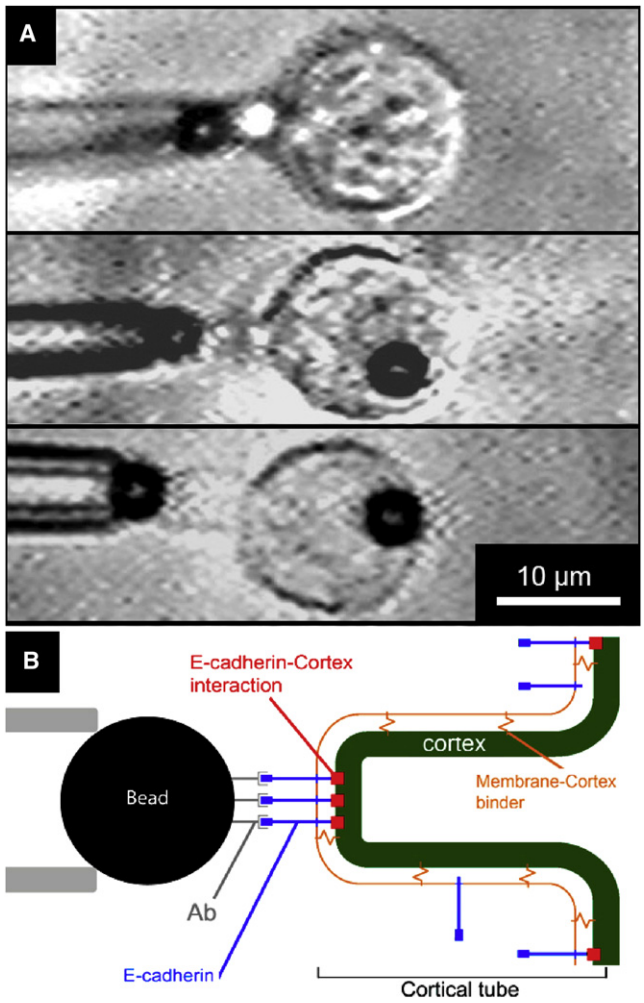

FIGURE 9 Videomicrographs (*A*) and schematic representation (*B*) of the cortical tubes extracted from Ecad cells/Ab-beads.

CONCLUSIONS

Membrane tube extrusion with S180 cells revealed the formation of two spatially different regions on the cell surface, characterized by different regimes of tube growth. The development of the initial fast extrusion velocity regime (FR) through extrusion cycles separated by short time intervals ($\Delta t \sim 30$ s) indicates the gradual and irreversible detachment of the plasma membrane from the cortical cytoskeleton and membrane accumulation at the extrusion site. Slow membrane flow (SR) indicates the persistence of an intact distal regime. For long intervals between extrusion cycles ($\Delta t \sim$ several minutes) the binders rebound and ν_n remains constant.

We also found that Ecad adhesion at the extrusion site altered cytoskeleton/membrane coupling, increasing resistance to membrane flow and tube extrusion. However, this effect was spatially limited to the cell/bead contact area, consistent with fine spatial regulation of cell adhesion to the microenvironment, enabling the cell to maintain local adhesion sites without having a major effect on the properties of the surrounding membrane and cortex, as required for many morphogenetic processes, including neuronal contact formation and maintenance, cell migration, and the formation of juncture belts in epithelial monolayers. We also observed an effect of aging on cells, which made it impossible for cells to give rise to more than two successive extrusions. The membrane/cortex interaction was restored remarkably quickly (in less than 30 s) in the case of Ecad-specific adhesion.

Our results show that Ecad homophilic interaction triggers the formation of a dense physical bridge between the membrane and the underlying cortex, modifying the membrane/cortex interaction and membrane flow properties. It has been suggested that Ecad adhesion plays a key role in morphogenesis by regulating cell surface tension (57). The machinery involved in this process is driven by the underlying cortical actin cytoskeleton and myosin-II-mediated contractility; however, further exploration of the links between Ecad-catenin complexes and the actin cytoskeleton is required (3,28). This study provides evidence that Ecad-mediated adhesion triggers tight high-energy membrane/cortical cytoskeleton coupling.

SUPPORTING MATERIAL

Four figures are available at http://www.biophysj.org/biophysj/supplemental/S0006-3495(09)00305-1.

The anti-Ecad mAb (7D9) was obtained from the Developmental Studies Hybridoma Bank, developed under the auspices of the National Institute of Child Health and Human Development and maintained by the Department of Biological Sciences, University of Iowa, Iowa City, Iowa. We thank Erdem Karatekin for fruitful discussions and constructive criticism.

This work was supported by the Centre National de la Recherche Scientifique, Institut Curie (Programme Incitatif et Coopératif, la Physique à l'Échelle de la Cellule). E.T. was supported by an Institut Curie fellowship. N.B. was supported by a fellowship (No. JR/MLD/MDV-P05/4) from the Association pour la Recherche sur le Cancer.

REFERENCES

1. Yagi, T., and M. Takeichi. 2000. Cadherin superfamily genes: functions, genomic organization, and neurologic diversity. *Genes Dev.* 14:1169–1180.
2. Nollet, F., P. Kools, and F. van Roy. 2000. Phylogenetic analysis of the cadherin superfamily allows identification of six major subfamilies besides several solitary members. *J. Mol. Biol.* 299:551–572.
3. Abe, K., and M. Takeichi. 2008. EPLIN mediates linkage of the cadherin catenin complex to F-actin and stabilizes the circumferential actin belt. *Proc. Natl. Acad. Sci. USA.* 105:13–19.
4. Adams, C. L., and J. W. Nelson. 1998. Cytomechanics of cadherin-mediated cell-cell adhesion. *Curr. Opin. Cell Biol.* 10:527–577.
5. Vleminckx, K., and R. Kemler. 1999. Cadherins and tissue formation: integrating adhesion and signaling. *Bioessays.* 21:211–220.
6. Gumbiner, B. M. 2005. Regulation of cadherin-mediated adhesion in morphogenesis. *Nat. Rev. Mol. Cell Biol.* 6:622–634.
7. Halbleib, J. M., and W. J. Nelson. 2006. Cadherins in development: cell adhesion, sorting, and tissue morphogenesis. *Genes Dev.* 20:3199–3214.
8. Murase, S., E. Mosser, and E. M. Schuman. 2002. Depolarization drives β-catenin into neuronal spines promoting changes in synaptic structure and function. *Neuron.* 35:91–105.
9. Yap, A. S., W. M. Brieher, M. Pruschy, and B. M. Gumbiner. 1997. Lateral clustering of the adhesive ectodomain: a fundamental determinant of cadherin function. *Curr. Biol.* 7:308–315.
10. Tsukita, S., M. Furuse, and M. Itoh. 1999. Structural and signalling molecules come together at tight junctions. *Curr. Opin. Cell Biol.* 11:628–633.
11. Takai, Y., and H. Nakanishi. 2003. Nectin and afadin: novel organizers of intercellular junctions. *J. Cell Sci.* 116:17–27.
12. Garrod, D. R., A. J. Merritt, and Z. Nie. 2002. Desmosomal adhesion: structural basis, molecular mechanism and regulation. *Mol. Membr. Biol.* 19:81–94, [Review].
13. Nose, A., A. Nagafuchi, and M. Takeichi. 1988. Expressed recombinant cadherins mediate cell sorting in model systems. *Cell.* 54:993–1001.
14. Shimoyama, Y., G. Tsujimoto, M. Kitajima, and M. Natori. 2000. Identification of three human type-II classic cadherins and frequent heterophilic interactions between different subclasses of type-II classic cadherins. *Biochem. J.* 349:159–167.
15. Foty, R. A., and M. S. Steinberg. 2005. The differential adhesion hypothesis: a direct evaluation. *Dev. Biol.* 278:255–263.
16. Chu, Y. S., O. Eder, W. A. Thomas, I. Simcha, F. Pincet, et al. 2006. Prototypical type I E-cadherin and type II cadherin-7 mediate very distinct adhesiveness through their extracellular domains. *J. Biol. Chem.* 281:2901–2910.
17. Adams, C. L., W. J. Nelson, and S. J. Smith. 1996. Quantitative analysis of cadherin-catenin-actin reorganization during development of cell-cell adhesion. *J. Cell Biol.* 135:1899–1911.
18. Adams, C. L., Y. -T. Chen, S. J. Smith, and W. J. Nelson. 1998. Mechanisms of epithelial cell-cell adhesion and cell compaction revealed by high-resolution tracking of E-cadherin-green fluorescent protein. *J. Cell Biol.* 142:1105–1119.
19. Linnemann, D., and E. Bock. 1989. Cell adhesion molecules in neural development. *Dev. Neurosci.* 11:149–173.
20. McLaughlin, S., J. Wang, A. Gambhir, and D. Murray. 2002. PIP(2) and proteins: interactions, organization, and information flow. *Annu. Rev. Biophys. Biomol. Struct.* 31:151–175.
21. Nebl, T., S. W. Oh, and E. J. Luna. 2000. Membrane cytoskeleton: PIP(2) pulls the strings. *Curr. Biol.* 10:351–354.
22. Sheetz, M. P. 2001. Cell control by membrane-cytoskeleton adhesion. *Nat. Rev. Mol. Cell Biol.* 2:392–396.
23. Sako, Y., A. Nagafuchi, S. Tsukita, M. Takeichi, and A. Kusumi. 1998. Cytoplasmic regulation of the movement of E-cadherin on the free cell surface as studied by optical tweezers and single particle tracking: corralling and tethering by the membrane skeleton. *J. Cell Biol.* 140:1227–1240.

24. Kusumi, A., K. Suzuki, and K. Koyasako. 1999. Mobility and cytoskeletal interactions of cell adhesion receptors. *Curr. Opin. Cell Biol.* 11:582–590.
25. Thery, M., V. Racine, A. Pepin, M. Piel, Y. Chen, et al. 2005. The extracellular matrix guides the orientation of the cell division axis. *Nat. Cell Biol.* 7:947–953.
26. Cuvelier, D., M. Thery, Y. S. Chu, S. Dufour, J. P. Thiery, et al. 2007. The universal dynamics of cell spreading. *Curr. Biol.* 17:694–699.
27. Krieg, M., Y. Arboleda-Estudillo, P. H. Puech, J. Kafer, F. Graner, et al. 2008. Tensile forces govern germ-layer organization in zebrafish. *Nat. Cell Biol.* 10:429–436.
28. Drees, F., S. Pokutta, S. Yamada, W. J. Nelson, and W. I. Weis. 2005. α-Catenin is a molecular switch that binds E-cadherin-β-catenin and regulates actin-filament assembly. *Cell.* 123:903–915.
29. Chu, Y. S., S. Dufour, J. P. Thiery, E. Perez, and F. Pincet. 2005. Johnson-Kendall-Roberts theory applied to living cells. *Phys. Rev. Lett.* 94, 028102.
30. Hochmuth, R. M., N. Mohandas, and P. L. Blackshear, Jr. 1973. Measurement of the elastic modulus for red cell membrane using a fluid mechanical technique. *Biophys. J.* 13:747–762.
31. Borghi, N., and F. Brochard-Wyart. 2007. Tether extrusion from red blood cells: integral proteins unbinding from cytoskeleton. *Biophys. J.* 93:1369–1379.
32. Waugh, R. E., and R. G. Bauserman. 1995. Physical measurements of bilayer-skeletal separation forces. *Ann. Biomed. Eng.* 23:308–321.
33. Hwang, W. C., and R. E. Waugh. 1997. Energy of dissociation of lipid bilayer from the membrane skeleton of red blood cells. *Biophys. J.* 72: 2669–2678.
34. Heinrich, V., A. Leung, and E. Evans. 2005. Nano-to-microscale mechanical switches and fuses mediate adhesive contacts between leukocytes and the endothelium. *J. Chem. Inf. Model.* 45:1482–1490.
35. Shao, J. Y., and R. M. Hochmuth. 1996. Micropipette suction for measuring piconewton forces of adhesion and tether formation from neutrophil membranes. *Biophys. J.* 71:2892–2901.
36. Schmidtke, D. W., and S. L. Diamond. 2000. Direct observation of membrane tethers formed during neutrophil attachment to platelets or P-selectin under physiological flow. *J. Cell Biol.* 149:719–730.
37. Hochmuth, F. M., J. Y. Shao, J. Dai, and M. P. Sheetz. 1996. Deformation and flow of membrane into tethers extracted from neuronal growth cones. *Biophys. J.* 70:358–369.
38. Li, Z., B. Anvari, M. Takashima, P. Brecht, J. H. Torres, et al. 2002. Membrane tether formation from outer hair cells with optical tweezers. *Biophys. J.* 82:1386–1395.
39. Raucher, D., T. Stauffer, W. Chen, K. Shen, S. Guo, et al. 2000. Phosphatidylinositol 4,5-bisphosphate functions as a second messenger that regulates cytoskeleton-plasma membrane adhesion. *Cell.* 100:221–228.
40. Berk, D. A., and R. M. Hochmuth. 1992. Lateral mobility of integral proteins in red blood cell tethers. *Biophys. J.* 61:9–18.
41. Brochard-Wyart, F., N. Borghi, D. Cuvelier, and P. Nassoy. 2006. Hydrodynamic narrowing of tubes extruded from cells. *Proc. Natl. Acad. Sci. USA.* 103:7660–7663.
42. Bennett, V. 1989. The spectrin-actin junction of erythrocyte membrane skeletons. *Biochim. Biophys. Acta.* 988:107–121.
43. Koppel, D. E., M. P. Sheetz, and M. Schindler. 1981. Matrix control of protein diffusion in biological membranes. *Proc. Natl. Acad. Sci. USA.* 78:3576–3580.
44. Friedlander, D. R., R. -M. Mege, B. A. Cunningham, and G. M. Edelman. 1989. Cell sorting-out is modulated by both the specificity and amount of different cell-cell adhesion molecules (CAMs) expressed on cell surfaces. *Proc. Natl. Acad. Sci. USA.* 86:7043–7047.
45. Nakagawa, S., and M. Takeichi. 1995. Neural crest cell-cell adhesion controlled by sequential and subpopulation-specific expression of novel cadherins. *Development.* 121:1321–1332.
46. Chu, Y. S., W. A. Thomas, O. Eder, F. Pincet, E. Perez, et al. 2004. Force measurements in E-cadherin-mediated cell doublets reveal rapid adhesion strengthened by actin cytoskeleton remodeling through Rac and Cdc42. *J. Cell Biol.* 167:1183–1194.
47. Lambert, M., F. Padilla, and R. M. Mege. 2000. Immobilized dimers of N-cadherin-fc chimera mimic cadherin-mediated cell contact formation: contribution of both outside-in and inside-out signals. *J. Cell Sci.* 113:2207–2219.
48. Hochmuth, R. M., and W. D. Marcus. 2002. Membrane tethers formed from blood cells with available area and determination of their adhesion energy. *Biophys. J.* 82:2964–2969.
49. Yamada, S., S. Pokutta, F. Drees, W. I. Weis, and W. J. Nelson. 2005. Deconstructing the cadherin-catenin-actin complex. *Cell.* 123:889–901.
50. Brochard-Wyart, F., and P. G. De Gennes. 2003. Unbinding of adhesive vesicles. *C.R. Phys.* 4:281–287.
51. Waugh, R. E., and R. M. Hochmuth. 1987. Mechanical equilibrium of thick, hollow, liquid membrane cylinders. *Biophys. J.* 52:391–400.
52. Herant, M., W. A. Marganski, and M. Dembo. 2003. The mechanics of neutrophils: synthetic modeling of three experiments. *Biophys. J.* 84: 3389–3413.
53. Drury, J. L., and M. Dembo. 2001. Aspiration of human neutrophils: effects of shear thinning and cortical dissipation. *Biophys. J.* 81:3166–3177.
54. Marcy, Y., J. Prost, M. F. Carlier, and C. Sykes. 2004. Forces generated during actin-based propulsion: a direct measurement by micromanipulation. *Proc. Natl. Acad. Sci. USA.* 101:5992–5997.
55. Gerbal, F., V. Laurent, A. Ott, M. F. Carlier, P. Chaikin, et al. 2000. Measurement of the elasticity of the actin tail of *Listeria monocytogenes*. *Eur. Biophys. J.* 29:134–140.
56. Landau, L. D., and E. M. Lifshitz. 1962. Course of Theoretical Physics, 3rd ed., Vol. 7: Theory of Elasticity. Pergamon Press, London, UK.
57. Lecuit, T., and P. F. Lenne. 2007. Cell surface mechanics and the control of cell shape, tissue patterns and morphogenesis. *Nat. Rev. Mol. Cell Biol.* 8:633–644.